

# LOSA-M2 aerosol Raman lidar

Yu.S. Balin, G.S. Bairashin, G.P. Kokhanenko, M.G. Klemasheva,  
I.E. Penner, S.V. Samoilova

**Abstract.** The scanning LOSA-M2 aerosol Raman lidar, which is aimed at probing atmosphere at wavelengths of 532 and 1064 nm, is described. The backscattered light is received simultaneously in two regimes: analogue and photon-counting. Along with the signals of elastic light scattering at the initial wavelengths, a 607-nm Raman signal from molecular nitrogen is also recorded. It is shown that the height range of atmosphere probing can be expanded from the near-Earth layer to stratosphere using two (near- and far-field) receiving telescopes, and analogue and photon-counting lidar signals can be combined into one signal. Examples of natural measurements of aerosol stratification in atmosphere along vertical and horizontal paths during the expeditions to the Gobi Desert (Mongolia) and Lake Baikal areas are presented.

**Keywords:** lidar, elastic and Raman scattering, atmosphere probing.

## 1. Introduction

Currently, most developed countries of the world use lidar complexes (located both within a country and beyond it) to implement national and international scientific programs of monitoring the optical and thermodynamic state of atmosphere. Examples are the Arctic High Spectral Resolution Lidar (the United States) [1] and SIBATA lidars of the NIES Network (Japan) in China, Korea, and Mongolia [2].

Moreover, ten years ago 19 European lidar stations from 11 countries were joined on the general methodological basis into the European Aerosol Research Lidar Network to monitor the spatial and temporal distribution of aerosol fields in atmosphere above the European territory [3]. Furthermore, the Southeast Asian Lidar Network for Atmospheric Studies [4], which combined research teams from China, Japan, and Korea, was organised to solve similar problems: study the transboundary transport of aerosol impurities caused by sandstorms in the Gobi and Takla-Makan deserts.

In terms of the development of these international integration processes, six research teams from Russia, Belarus, and Kyrgyzstan developed the Commonwealth of Independent States Lidar Network (Cis-LiNet) in 2004 [5], which is extended from Minsk to Vladivostok.

The lidars of all these networks are large stationary instrumental complexes, equipped with different types of laser trans-

mitters, photodetectors, and detection channels for multiwave elastic and Raman scattering. As was correctly noted in [3], to organise joint operation of lidars, it is primarily necessary to perform their high-quality mutual calibration; this is fairly difficult to do because of their location at large distances from each other.

The Micro-Pulse Lidar Network MPL-Net, which was developed to monitor tropospheric aerosol [6], does not solve this problem in full measure, because it controls the optical parameters of atmosphere at only one wavelength. In this context, an urgent problem is to develop small transportable lidars, which are similar to large complexes in measurement technologies and, at the same time, allow one to perform joint efficient measurements in different regions.

A compact multiwave LOSA-M2 aerosol Raman lidar was developed at the Zuev Institute of Atmosphere Optics in 2008. One of its main purposes was to perform field expedition studies of the near-Earth and boundary layers, troposphere, and stratosphere in different regions. In this paper, we describe the characteristics of this lidar (which is a modification of the LOSA-MS lidar [7]).

## 2. Lidar design and optical scheme

The compact LOSA-M2 lidar is shown in Fig. 1a. Its technical characteristics are as follows.

### Laser LS-2135

Energy/mJ at the wavelengths:	
1064 nm . . . . .	340
532 nm . . . . .	170
Pulse width/ns . . . . .	10–12
Pulse repetition rate/Hz . . . . .	10
Beam divergence/mrad . . . . .	2.5
Beam diameter/mm . . . . .	8

### Optical receiving system

Diameter of the main telescope/mm . . . . .	250
Focal length/mm . . . . .	1000
Diameter of the near-field telescope/mm . . . . .	50
Focal length/mm . . . . .	200
Field of view of the telescope/mrad . . . . .	1.5
Filter bandwidth/nm . . . . .	2–4

### Analogue–digital converter LAn10-12USB

Number of analogue inputs . . . . .	2
Maximum discretisation frequency/MHz . . . . .	100
Input resistance/ $\Omega$ . . . . .	50
Input-voltage ranges/V . . . . .	$\pm 2, \pm 1, \pm 0.4, \pm 0.2$
Resolution/bit . . . . .	12

Yu.S. Balin, G.S. Bairashin, G.P. Kokhanenko, M.G. Klemasheva,  
I.E. Penner, S.V. Samoilova V.E. Zuev Institute of Atmosphere  
Optics, Siberian Branch, Russian Academy of Sciences, pl. Akad.  
Zueva 1, 634021 Tomsk, Russia; e-mail: balin@iao.ru

Received 22 June 2011

Kvantovaya Elektronika 41 (10) 945–949 (2011)

Translated by Yu.P. Sin'kov



Figure 1. Transceiver of the lidar LOSA-M2.

*Pulse counter PhCount-2USB*

Number of channels . . . . .	2
Count rate/MHz . . . . .	100
Spatial resolution/m. . . . .	1.5
Input resistance/ $\Omega$ . . . . .	50

The LOSA-M2 lidar is intended for remote atmosphere probing under field conditions. This imposes rather strict requirements to its design in order to preserve optical alignments during long-term transportations and to protect it from the influence of unfavourable weather factors. Therefore, all basic units of the transceiver (laser, telescopes, collimator, and other optical elements) are mounted at both sides of a unified platform, which can be rotated in the fixing of the rotational device. The platform is a frame with a volume profile, which stiffens it additionally. Heating elements and fans, which maintain the necessary working temperature of the lidar transceiver (independent of the external conditions), are uniformly distributed inside the frame. The transceiver is placed in a thermally insulating housing. Additional hoods are used to eliminate direct exposure to sunlight. The design of the rotational device makes it possible to fix the transceiver block on the platform of mobile carriers in fixed positions. In addition, there is a possibility of jointing this block with the scanning column and obtain spatial cuts of aerosol fields in both vertical and horizontal planes.

The general principle of lidar operation is conventional. Atmosphere is probed by pulsed laser radiation at wavelengths of 1064 and 532 nm. The light backscattered by the atmosphere is collected by mirror telescopes and recorded by photodetectors with subsequent digitisation of the signals and processing and visualisation of the data obtained by an instrumental program complex based on a high-efficiency notebook with an external interface protocol through USB ports.

At the same time, in comparison with most of stationary laser complexes, the LOSA-M2 lidar has a number of technological features related to the specific atmospheric problems to be solved: extended height probing range (from the near-Earth layer to stratosphere, 15–30 km) and necessity of day-and-night probing. These conditions determine the require-

ments to the lidar transceiver design. Original schemes and methodical solutions have been developed and implemented to solve these problems. The transceiver optical scheme is based on two (short- and far-field) receiving telescopes, with alternate extraction of optical signals from them to the same photodetectors. The signals are simultaneously recorded in two regimes, analogue and photon-counting. Along with the elastic scattering at the initial wavelengths, the scattered radiation contains a 607-nm Raman line of molecular nitrogen. Since this line is characterised by a backscattering cross sections that is several orders of magnitude smaller, it is recorded by photodetectors operating in the photon-counting regime. An additional channel is also used to record elastic scattering at a wavelength of 532 nm (also in the photon-counting regime); this approach makes it possible to increase the data probing range by a factor of 2–3 when accumulating signals.

The optical scheme of the lidar is shown in Fig. 2. The lidar transmitter consists of a solid-state Nd:YAG laser (1) (LS2135, LOTIS-TII, Belarus), which emits along one axis at wavelengths of 1064 and 532 nm. The laser radiation is expanded by an achromatic three-lens collimator (2), which makes it possible to reduce the angle of divergence of the beam to 0.5 mrad in the UV and IR ranges [8]. The main receiving Cassegrain telescope (3) (mirror diameter 250 mm, focal length 1 m) is used to receive the far-field radiation, and an off-axis parabola (4) (diameter 50 mm, focal length 200 mm) receives the near-field radiation at distances smaller than 1.5 km. There is a diaphragm (5) at the focus of the main telescope, which limits the field of view to 1 mrad. The radiation from the near-field receiver is fed at the same point using an optical fibre (6). A mirror chopper (7) rotates with a frequency of 10 Hz (synchronised with the laser pulse repetition frequency); it allows one to feed successively the radiation received by both telescopes to the photodetection channels. A lens (8) forms a parallel beam 16 mm in diameter.

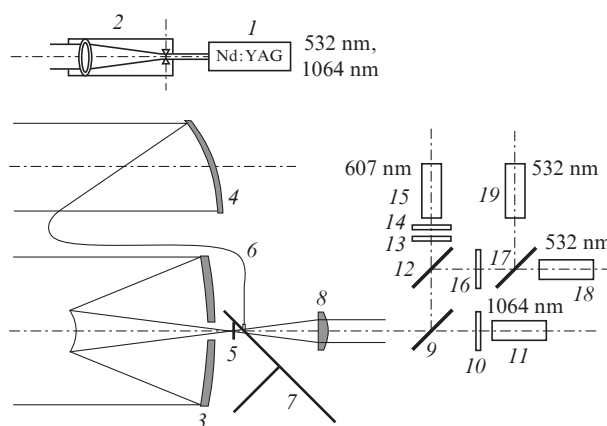


Figure 2. Optical scheme of the lidar.

The radiation received is separated over wavelengths using interference optics. The first dichroic mirror (9) transmits IR radiation (1064 nm) and reflects off visible light. IR radiation passes through an interference filter (IF) (10) and is detected by a C30956E-TC 11 avalanche photodiode (Perkin&Elmer).

A dichroic mirror (12) transmits 607-nm radiation, which passes through an IF (13) and a band filter (14) (the latter

additionally cuts off radiation at  $\lambda = 532$  nm) to arrive at an H7155P-21 photomultiplier tube (PMT) (Hamamatsu) (15), operating in the photon-counting regime. Attenuation of the excitation line using cut-off filters in combination with the IFs, mounted on each photodetector, allows one to suppress the excitation radiation (532 nm) in the Raman channels by six orders of magnitude for 607-nm signals. The 532-nm radiation reflected from a mirror (12) passes through an IF (16) and is split by a glass plate (17) in the ratio 1:20 to arrive at two PMTs: FEU-84 (18), which operate in the current regime, and H5783P (Hamamatsu) (19), which operates in the photon-counting regime.

Elastic scattering signals at  $\lambda = 532$  nm are recorded in the current regime by a photo module FM-1 (Zuev Institute of Atmosphere Optics, Tomsk). The photo module FM-1 for detecting pulsed light signals against an intense illumination background has been developed based on PMT-84 and an original specialised power supply. A push–pull converter with independent excitation, operating at a frequency of 150 kHz, feeds a full-wave multistage voltage multiplier through a transformer to form a dc voltage across the dynodes, which is independent of the illumination background. To exclude PMT failure, a locking voltage is constantly applied at a high average anode current to the modulator. At the instant when the laser lamp is ignited, a gate based on optical relay unlocks the PMT for a time that is chosen depending on the desired lidar range. The photo module must be fed by an external voltage of 24 V. The implemented version of voltage distribution between dynodes using a multistage voltage multiplier provides a constant voltage across dynodes at any illumination background levels and, therefore, a constant PMT multiplication factor. When the PMT is shaded, power is not consumed in the supply circuit, due to which one can do without a heat sink, and the power supply can be made more compact. Tests showed that in the illumination range up to a level corresponding an average anode current of 10 mA, the PMT gain is invariable in the range of three orders of the light characteristic.

Analogue signals are digitised by a 12-bit ADC (LAN10-12USB-U, Rudnev–Shilyaev closed joint-stock company) with a spatial resolution to 1.5 m. A 1064-nm signal is recorded by an APD-30956-TE photodetection module (developed at the Institute of Physics, National Academy of Sciences of Belarus), which includes a C30956E avalanche photodiode (Perkin& Elmer) with a microcooler and an amplifier. Raman signals are recorded by H5783P photodetection modules (Hamamatsu) with amplifiers and a PhCount-2USB pulse counter (developed at the Zuev Institute of Atmosphere Optics), which makes it possible to count photons with a frequency up to 100 MHz and a spatial resolution of 1.5 m. To compare correctly the Raman and elastic scattering signals, some part (about 5%) of 532-nm radiation is branched into similar counting channels. At a laser pulse repetition rate of 10 Hz and 30-min photon accumulation, Raman signals of molecular nitrogen are reliably recorded up to the tropopause height in the absence of cloudiness. Note that the systems of signal detection are located directly in the transceiver housing, and the communication lines transfer digital information.

### 3. Field tests of lidars

In this section we report as examples the results of separate lidar measurements, which were performed during the complex ‘Baikal’ and ‘Mongolia’ expeditions.

Let us first consider the specific features of the formation of the total lidar signal (which was obtained by the two receiving telescopes), as well as the analogue and photon-counting signals. The use of near- and far-field receiving telescopes allows one to cover a large dynamic range of variation in lidar signals during atmosphere probing, thus covering maximally the lidar-controlled space.

Figure 3 shows the geometric overlap function (form factor) of the emitter diagram and the field of view of the near- and far-field receiving telescopes. The complete intercept of single backscattering for the near-field telescope begins practically with 80 m, whereas for the main far-field telescope this occurs beginning with 900 m. Since the aperture area of the near-field telescope is smaller by a factor of 20 than that of the main telescope, the backscattered light flux received by the near-field telescope (this flux is most intense at small distances) does not overload the photodetectors. The latter work in the linear range of light characteristics for both the near- and far-field signals. An instrumental program complex is used to synchronise laser pulses, and the chopper is successively switched between the light fluxes from the near- and far-field telescopes. In addition, the signals from the photodetectors of three spectral channels (for wavelengths of 1064, 532, and 607 nm) are recorded separately into near- and far-field data files. During the subsequent preliminary treatment the complete profile of received signals is reconstructed along the entire probing path.

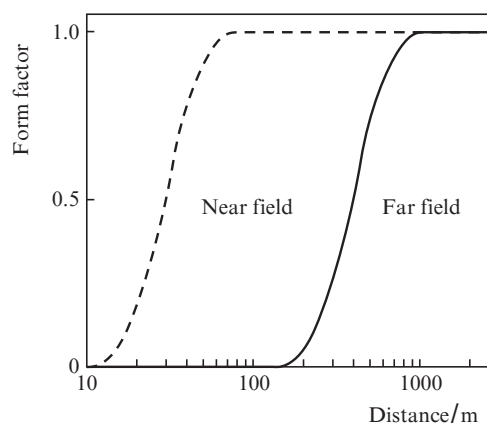
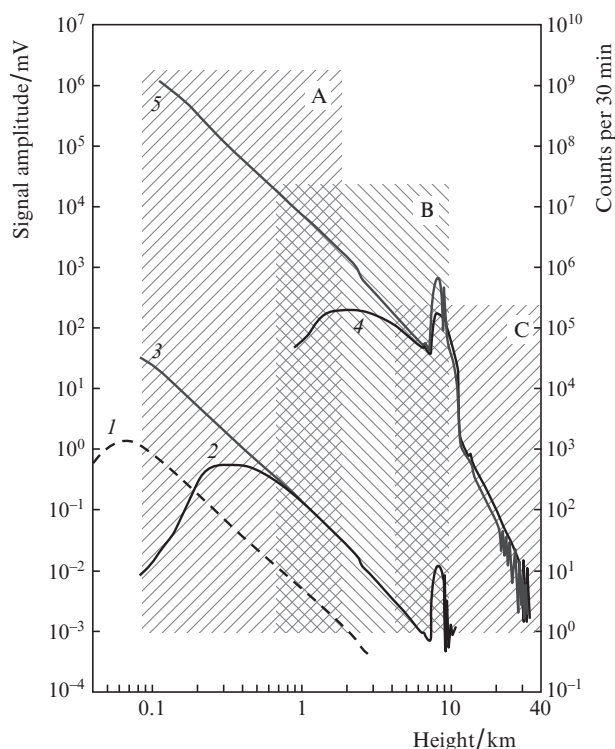


Figure 3. Lidar form factor.

We will illustrate this technique by an example of specific implementation in a session of vertical atmosphere probing in the Gobi Desert in July, 2008 (‘Mongolia-08’ expedition). The session was performed during the hours of darkness, and we could use photodetectors operating in the photon-counting regime. Figure 4 shows implementations of signals for the 532-nm spectral channel: curves (1) and (2) (averaged over the settled period of photon accumulation,  $\sim 30$  min) from the analogue photodetectors of the near- and far-field receiving telescopes respectively, and curve (4) from the photodetector operating in the photon-counting regime. Figure 4 shows also the diagrams of linear ranges of lidar signals (hatched areas): (A) for a near-field signal [from 90 m, in correspondence with the form factor (Fig. 3), to no more than 2000 m at a signal-to-noise ratio exceeding 1]; (B) for a far-field signal (from 900 to  $\sim 12000$  m); and (C) for a far-field signal, but from the photodetector operating in the photon-counting regime. The



**Figure 4.** Implementations of signals in the multichannel receiving system of the LOSA-M2 lidar at a probing wavelength of 532 nm. Left ordinate axis: (1) near-field analogue signal, (2) far-field analogue signal, and (3) reconstructed signal with the analogue channels. Right ordinate axis: (4) far-field photon-counting signal and (5) reconstructed analogue–photon-counting signal.

linear range of accumulated signal for the latter is from  $\sim 4$  to  $\sim 35$  km. The lower limit of the height range for the counting channel is determined by the limitations on the count rate at an intense signal. In the overlap areas of these diagrams (double hatching in Fig. 4), amplitude matching of signals is performed, and the average proportionality factor between them is determined by the least-squares method. For example, the near-field analogue signal is multiplied by this factor and is matched with the far-field signal in their overlap region. The thus reconstructed signal from the analogue channel is shown in Fig. 4 [curve (3)]. A similarly reconstructed signal from the analogue photodetector is recounted per number of counts and is matched with the signal of the photodetector operating in the photon-counting regime [curve (5)].

Thus, the received signals can be reconstructed over the vertical probing path (0.1–30 km) in a dynamic range up to nine or ten orders of magnitude, whereas the linearity of the light characteristic of individual photodetectors has a limited dynamic range, which generally does not exceed three orders of magnitude. Figure 5 shows a continuous profile of the backscattering coefficient, which was reconstructed from the above-considered implementations of signals using the techniques applied by us for aerosol Raman lidars of this type [9]. The errors in measuring the backscattering coefficient are indicated by horizontal bars. The profile exhibits characteristic aerosol layers of atmosphere stratification from the near-Earth layer ( $\sim 100$  m) to the lower layers of stratosphere ( $\sim 25$  km). These are the pronounced boundary layer to a height of 2.5 km; a thin layer beneath the clouds at a height of 6.5 km; and pronounced aerosol layers observed at heights of 13–14 km,

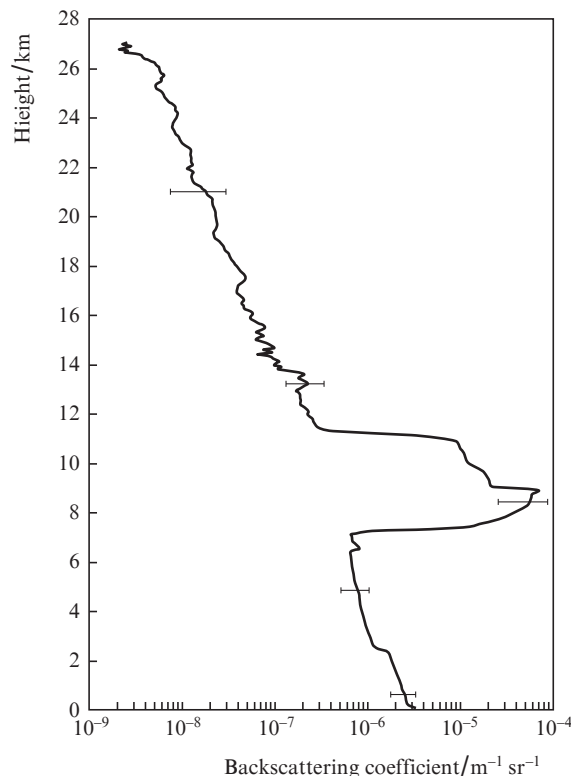


**Figure 5.** Profile of the aerosol backscattering coefficient, reconstructed from the lidar signal presented in Fig. 4.

despite the presence of multilayer cloudiness of the upper layer at heights from 7 to 11 km with an optical thickness reaching unity. These aerosol layers, as was noted in [10], are traces of aerosol perturbation of the lower stratosphere by eruption products from the Okmok volcano.

An example of atmosphere probing along horizontal paths above a flat underlying surface are the lidar data obtained by us in the Baikal Lake basin during the ‘Baikal-08’ expedition. The probing was performed along a horizontal path across the Baikal Lake (Fig. 6): from the testing area of the Buryat Scientific Centre, Siberian Branch, Russian Academy of Sciences (BSC SB RAS) in Boyarsk settlement (where the lidar



**Figure 6.** Atmosphere probing by the lidar LOSA-M2 above Lake Baikal at the stationary testing area in Boyarsk (Department of Physical Problems of BSC SB RAS).

was located) to the opposite shore near Bolshoe Goloustnoe settlement. Figure 7b shows a signal from a photodetector operating in the photon-counting regime in the 532-nm channel, which is the result of matching near- and far-field signals. The finite point of the path, which is spaced by 52 km, contains a pronounced reflection peak from the mountain ridge on the opposite shore. Figure 7a presents a profile of aerosol attenuation coefficient (with rms deviations indicated), which was reconstructed from this smoothed signal. One can see well increased aerosol content at distances of up to 10 km from both shores and a wavy character of layers distribution above the Lake Baikal water surface. We revealed a similar spatial structure during lidar ship studies of aerosol fields in the atmosphere above Lake Baikal [11]; however, it took several hours to obtain one transverse cut in those studies. In this probing session the cut was obtained for a time of signal accumulation, i.e., for  $\sim 25$  min.

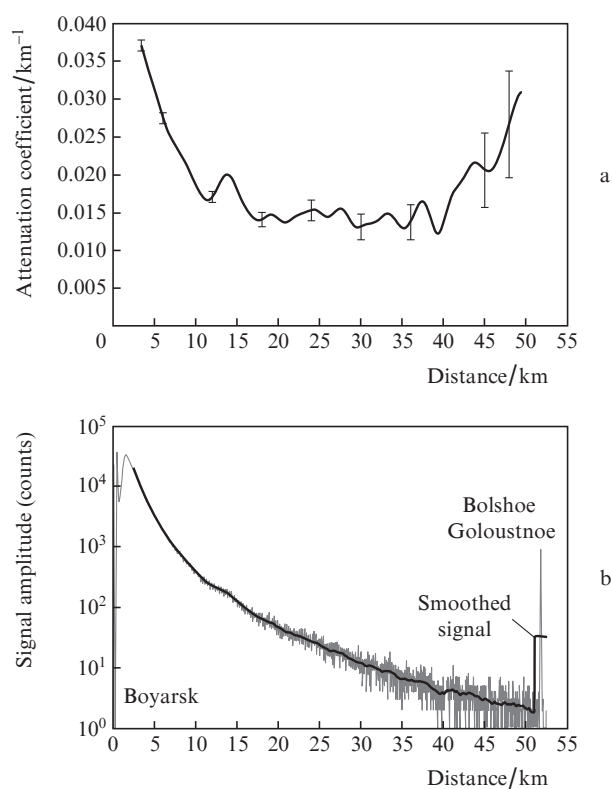


**Figure 7.** (a) Profile of the attenuation coefficient and (b) photon-counting signal (in counts per 25 min), according to probing data along a horizontal path above Lake Baikal.

#### 4. Conclusions

A compact expedition LOSA-M2 aerosol Raman lidar was developed, which makes it possible to monitor the optical state of atmosphere from the near-Earth layer to the stratosphere in one measurement cycle. This dynamic range is obtained due to the application of near- and far-field receiving telescopes, as well as analogue and counting-photon regimes for detecting lidar signals.

The efficiency of the LOSA-M2 lidar was proven in a number of Russian and international expeditions. The compact LOSA-M aerosol Raman lidar was awarded a diploma of a winner of the competition carried out by the Laser Asso-

ciation of Russia at the International Exhibition 'Photonics-09' in 2009 as one of the best Russian developments in the field of laser instrument making.

**Acknowledgements.** This study was supported in part by the Russian Foundation for Basic Research (Grant No. 10-08-00347-a), the Presidium of the Russian Academy of Sciences (Project No. 4.13), and the Ministry of Education and Science of Russian Federation (State Contract Nos 14.740.11.0204, 02.740.11.0674, and 16.518.11.7067).

#### References

1. Razekov I.A., Eloranta E.W., Hedrick J.P., Holz R.E., Kuehn R.E., Garcia J.P. *Proc. 21st Int. Laser Radar Conf. (ILRC21)* (Quebec, Canada, 2002) p. 57.
2. <http://www.sibata.co.jp>
3. Bösenberg J., Ansmann A., Baldasano J., Balis D., Böckmann C., Calpini B., Chaikovskiy A., Flamant P., Hagard A., Mitev V., Papayannis A., Pelon J., Resendes D., Schneider J., Spinelli N., Trickle T., Vaughan G., Visconti G., Wiegner M. *Advances in Laser Remote Sensing: Selected Papers 20th Int. Laser Radar Conf. (ILRC)* (Vichi, France, 2000) p. 155.
4. Murayama T., Sugimoto N., Matsui I., Lio Zh., Sakai T., Shibata T., Iwasaka Y., Won J.G., Yoon S.C., Li T., Zhou J., Hu H. *Advances in Laser Remote Sensing: Selected Papers 20th Int. Laser Radar Conf. (ILRC)* (Vichi, France, 2000) p. 169.
5. Chaikovskii A.P., Ivanov A.P., Balin Yu.S., El'nikov A., Tulinov G.F., Plyusnin I.I., Bukin O.A., Chen B.B. *Opt. Atmos. Okeana*, **18**, 1066 (2005).
6. Welton E.J., Campbell J.R., Berkoff T.A., Spinhime J.D., Tsay S.Ch., Holben B., Shiobara M. *Proc. 21st Int. Laser Radar Conf. (ILRC21)* (Quebec, Canada, 2002) p. 285.
7. Bairashin G.S., Balin Yu.S., Ershov A.D., Kokhanenko G.P., Penner I.E. *Opt. Eng.*, **44** (7), 071209-1 (2005).
8. Kokhanenko G.P., Makogon M.M., Ponomarev Yu.N., Rynkov O.A., Simonova G.V. Patent No. 2009129019/22(040351) (2009).
9. Samoilova S.V., Balin Yu.S., Kokhanenko G.P., Penner I.E. *Opt. Atmos. Okeana*, **22**, 344 (2009).
10. Zuev V.V., Balin Yu.S., Bukin O.A., Burlakov V.D., Dolgii S.I., Kabashnikov V.P., Nevzorov A.V., Osipenko F.P., Pavlov A.N., Penner I.E., Samoilova S.V., Stolyarchuk S.Yu., Chaikovskii A.P., Shmirko K.A. *Opt. Atmos. Okeana*, **22**, 450 (2009).
11. Balin Yu.S., Ershov A.D., Penner I.E. *Opt. Atmos. Okeana*, **16**, 587 (2003).